JOURNAL OF CATALYSIS **171,** 77–84 (1997)
ARTICLE NO. CA971779

Kinetics of Hydro-isomerization of *n*-Hexane over Platinum Containing Zeolites

A. van de Runstraat, J. A. Kamp, P. J. Stobbelaar, J. van Grondelle, S. Krijnen, and R. A. van Santen

Department of Inorganic Chemistry and Catalysis, Faculty of Chemical Engineering, Eindhoven University of Technology, P.O. Box 513, 5600 MB Eindhoven, The Netherlands

Received November 27, 1996; revised March 1, 1997; accepted May 20, 1997

Kinetic hydro-isomerization experiments at atmospheric pressure using *n*-hexane as reactant were performed. Four zeolites with different pore structures but intrinsically equal acid strength (mordenite, ZSM-5, ZSM-22, and β) were used. Adsorption and diffusion effects were found to mainly determine the differences in activity of these zeolites. The general observation is that the higher the adsorption enthalpy of *n*-hexane, the higher the activity per acid site and the lower the activation energy. The latter effect is not very pronounced when the order of reaction in *n*-hexane is low. The true activation energy of isomerization with respect to the adsorbed alkoxy state is found to be approximately 125 kJ/mol. ZSM-22 and mordenite were both relatively inactive compared to the other zeolites. In the case of ZSM-22 this was due to pore-mouth catalysis resulting in a 5 to 20% usage of the acid sites. The relatively low activity of mordenite occurs since two-thirds of the acid sites, those located in the side-pockets, are not accessible to *n*-hexane.

1. INTRODUCTION

In this paper we will report the results of a study of the catalytic activity of acidic zeolites. It will be determined whether differences are solely due to differences in intrinsic zeolite proton properties or differences in adsorption characteristics. We used the hydro-isomerization of *n*-hexane as a model reaction since its low deactivation rate enabled study of the reaction under true steady-state conditions. Catalysts had to be chosen such that the platinum function was not rate determining. Hexane was chosen as reactant because of its low cracking rate. The rate of isomerization could therefore be approximated by the rate of *n*-hexane conversion.

Four zeolites with a Si/Al ratio larger than 10 were chosen. The catalysts had the same intrinsic acid strength, as determined by ^{1}H NMR and IR spectroscopy. Therefore, comparison of their activities normalized per acid site was useful. From the data obtained on the optimized ("key") samples an intrinsic activation energy of isomerization in zeolites could be deduced.

The hydro-isomerization mechanism can be divided in (de)hydrogenation, protonation and isomerization steps. This bifunctional mechanism is given schematically in Fig. 1 (1). These reactions take place in the adsorbed state. According to Kazansky, adsorption of an alkene to an acid site of a zeolite gives an alkoxy species (2, 3). This species is characterized by a covalent bond between an oxygen atom from the zeolite lattice and a carbon atom of the alkene. The elementary isomerization reaction step involves in this case a carbenium ion-like transition state; the *n*-alkoxy species are the stable intermediates.

After a short summary of current thinking in hydro-isomerization kinetics, details of the experiments and their results will be provided. Under Discussion we will evaluate the results of optimizing the platinum content and the resulting "key" samples. The relation between performance of the zeolites and their adsorption behavior will be highlighted.

2. METHODS

A Summary of Hydro-isomerization Kinetics

When it is assumed that the isomerization reaction step is rate determining (ideal bifunctional behavior) and the hydrocarbon concentrations inside the zeolite are in equilibrium with the gas phase, the overall rate of isomerization is given by (4)

$$R = k_{\text{iso}} \frac{K_{\text{dehydr}} \cdot K_{\text{prot}} \cdot \left(\frac{p_{n\text{C}_6}}{p_{\text{H}_2}}\right)}{1 + K_{\text{dehydr}} \cdot K_{\text{prot}} \cdot \left(\frac{p_{n\text{C}_6}}{p_{\text{H}_2}}\right)} \approx k_{\text{iso}} \left(K_{\text{dehydr}} \cdot K_{\text{prot}} \cdot \left(\frac{p_{n\text{C}_6}}{p_{\text{H}_2}}\right)\right)^{\alpha}, \quad [1]$$

in which R is the rate of reaction, K_{dehydr} is the equilibrium constant of dehydrogenation, K_{prot} is the equilibrium constant of protonation, k_{iso} is the rate constant of isomerization, $p_{n\text{C}_6}$ is the partial pressure of *n*-hexane, and p_{H_2} is the partial pressure of hydrogen. The order of reaction α is equal to or smaller than 1.

0021-9517/97 $25.00

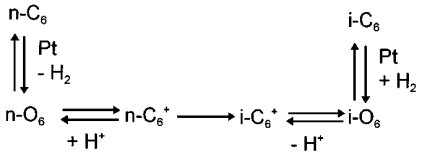

FIG. 1. Schematic representation of Weisz' bifunctional mechanism. *n*-C_6, *n*-hexane; *n*-O_6, *n*-hexene; *n*-C_6^+, *n*-carbenium ion; *i*-C_6^+, iso-carbenium ion; *i*-O_6, iso-hexene; *i*-C_6, iso-hexane.

When the zeolite micropore is almost completely covered with reactant, at high pressure or when a long alkane is used, Eq. [1] is no longer valid (5, 6). Then an expression as proposed by Steijns and Froment applies (5). This expression implies no equilibrium between hydrocarbons in the micropores and gas phase. The high micropore filling causes severe diffusion inhibition. The general form of this expression is

$$R = k_{\text{iso}} \frac{\text{PAR}(1) \cdot p_{n\text{-alkane}}}{p_{\text{H}_2} + \text{PAR}(2) \cdot p_{\text{H}_2} \cdot p_{n\text{-alkane}} + \text{PAR}(3) \cdot p_{n\text{-alkane}}}, \quad [2]$$

in which PAR(1), PAR(2), and PAR(3) are parameters consisting of equilibrium and adsorption constants. The term $\text{PAR}(3) \cdot p_{n\text{-alkane}}$ represents Langmuir adsorption of product alkanes. This equation has been confirmed for *n*-decane isomerization over a Pt/USY catalyst (6).

Expected orders at different conditions can be found in Table 1. We have developed a kinetic modeling scheme that reproduces the two extreme situations and enables simulations in the intermediate regime (7). When one takes the derivative of the natural logarithm of Eq. [1] toward the reciprocal of the temperature, one obtains (8)

$$E_{\text{act, iso}} = E_{\text{act, app}} + (1 - \theta_{n\text{-alkoxy}}) \cdot \left[-\Delta H_{\text{prot, ads}} - \Delta H_{\text{ads, } n=C_6} + \Delta H_{\text{dehydr}} \right], \quad [3]$$

in which $E_{\text{act, app}}$ is the apparent activation energy, $E_{\text{act, iso}}$ is the activation energy of *n*-alkoxy isomerization, ΔH_{dehydr} is the enthalpy of dehydrogenation, $\Delta H_{\text{prot, ads}}$ is the protonation enthalpy (alkoxy formation) from the adsorbed state, and $\Delta H_{\text{ads, } n=C_6}$ is the adsorption enthalpy of *n*-hexene. In this equation, the protonation enthalpy of hexene from the gas phase (actually, *n*-alkoxy formation) is expressed as the sum of $\Delta H_{\text{prot, ads}}$ and $\Delta H_{\text{ads, } n=C_6}$. It is assumed that the adsorption enthalpies of *n*-hexene and *n*-hexane are equal, which is a reasonable assumption (9, 10).

Substitution of Eq. [3] into Eq. [1] allows for the substitution of $(1 - \theta_{n\text{-alkoxy}})$ by α. Equation [3] will be used to determine the true activation energy of isomerization from experimental data. The values used for ΔH_{dehydr} and $\Delta H_{\text{prot, ads}}$ are respectively -114.8 and 80 kJ/mol. The first value has been obtained from thermodynamics (11). The latter value is a computed value (12).

TABLE 1

Expected Orders of Reaction under Different Conditions

		Equation [1]		Equation [2]	
$p_{n\text{-alkane}}$	p_{H_2}	*n*	*m*	*n*	*m*
High	High	Invalid		0	−1
High	Low			0	0
Low	High	α	$-\alpha$	1	−1
Low	Low	1	−1		

Note. *n*, order in *n*-alkane; *m*, order in hydrogen.

TABLE 2

Pore Structures of Zeolites Chosen

	One-dimensional	Three-dimensional
Medium pore	ZSM-22	ZSM-5
Large pore	Mordenite	β-Zeolite

Catalyst Treatment

Four zeolites were used that were representative of four prototype pore structures (Table 2). The Naβ-zeolite, NaZSM-5, and NaZSM-22 samples were kindly donated by Exxon Chemicals in Machelen, Belgium. The Na-mordenite was kindly donated by Shell Research and Technology Centre in Amsterdam, The Netherlands.

Conversion to the protonated forms was carried out through ammonium nitrate exchange and subsequent decomposition in nitrogen at 783 K and calcination at 773 K. Platinum loading of the zeolites was then performed by ion exchange with a platinum tetra-ammonium hydroxide solution. The filtrate was checked for platinum by UV–VIS to establish the true loading of the zeolite (13). The dried sample was then treated in one of the following ways:

(a1) Calcination at 723 K, reduction at 673 K and passivation at room temperature. Such a sample is referred to as an *ex situ pretreated* sample.

(a2) The pure *ex situ* pretreated sample was embedded in a silica matrix (Aerosil Degussa 380) by making a gel in which the zeolite particles were dispersed. Such a sample is referred to as an *embedded* sample.

(b) In case of a sample that was *pretreated in situ*, calcination and reduction were performed inside the reactor.

Sieve fractions of 125–500 μm were used in the reactor.

Catalyst Characterization

Acidity. The most important characteristics of the zeolites in the acidic form are given in Table 3. Two types of IR spectra were recorded as published by Jänchen *et al.* (14).

TABLE 3

Results of Characterization of the Acidic Zeolites Used

Analysis	HMOR	HBEA	HTON	HMFI
IR: ν(OH) [cm^{-1}]:	3608	3609	3600	3611
$\Delta\nu$ CD_3CN [cm^{-1}]:	1069	1078	1072	1073
^{1}H NMR, δ [ppm]:	4.1	4.3, 5.1	4.4	4.2
^{27}Al NMR, δ [ppm]:	−1.0, 54.5	−0.9, 53.4	53.4	−1.0, 55.2
$Si/Al_{framework}$ ratio[a]	12.5	17.0	44.7	40.7
$-\Delta H_{ads}$ [kJ/mol]	71.9	70	81.5	82

[a] Determined by ^{29}Si MAS NMR.

Both the frequency of the OH stretch vibration and its shift upon acetonitrile adsorption are a measure of intrinsic Brønsted acid strength. Since the shift always results in two broad bands, the shift (in cm^{-1}) based on the weighted average of these new bands is given. The higher the position of the OH peak and the smaller the shift upon acetonitrile adsorption, the lower the acid strength per proton.

Since the ^{1}H chemical shift for the acid sites and the OH stretch vibrations as well as the shift upon acetonitrile adsorption were the same for all zeolites used it may be concluded that they all had the same acid strength.

Crystal size and pore volume. The crystal size was determined by SEM. The mordenite and β-zeolite samples consisted of agglomerated crystals. The mordenite agglomerates were up to 20 μm in size and the zeolite β agglomerates up to 200 μm. We learned an important feature of mordenite by comparing the BET pore volume (0.2 ml/g) and *n*-hexane adsorption capacity (0.07 ml/g). These figures may indicate that only one-third of the sites inside the mordenite pores can be reached by *n*-hexane.

Calorimetry. The ΔH_{ads} values given in Table 3 are the calorimetrically measured heats of adsorption of *n*-hexane. The uncertainty of these values is less than 1 kJ/mol. Generally, a smaller pore size led to higher adsorption enthalpy. The heat of adsorption of β-zeolite is relatively low. An extrapolation of Configurational-Bias Monte Carlo calculations on all-silica β-zeolite confirmed the value of approximately 70 kJ/mol (15), which is probably due to the low density of β (16, 17). The value of ZSM-22 was not measured here but was taken from results of Eder (18).

Platinum function. In addition to hydrogen chemisorption, we used liquid phase hydrogenation experiments of 1-hexene to characterize the platinum particles. The results of both methods obtained on some representative samples are given in Table 4. A quasi turnover frequency ($qTOF_{Pt}$) is calculated by taking into account all platinum atoms present. X_{dev} stands for the conversion level of deviation from the straight line of conversion versus time. This level is a measure of mass-transfer limitations within the zeolite. Mass-transfer limitations of 1-hexene play a larger role when the points deviate at a conversion lower than approximately 80% (19).

The Kinetic Experiments

Equipment. *n*-Hexane (Acros 99+% purity), delivered by a HP1050 HPLC pump, was evaporated into flowing hydrogen or a hydrogen/nitrogen mixture. The gas flows were controlled by thermal mass-flow controllers. The mixture was then flowed through a fixed-bed, continuous flow reactor at atmospheric pressure. Quartz reactors with an internal diameter of 4 and 8 mm were used. Reaction products were analyzed on-line using a HP5890 Series II gas chromatograph equipped with a FID detector and a Chrompack fused silica column with a Al_2O_3/KCl coating.

Conditions. Standard conditions were 513 K, 0.03 ml/min liquid flow of *n*-hexane, and a 145 Nml/min flow of hydrogen. The WHSV was tuned by using an amount of catalyst (between 50 and 200 mg) which yielded a conversion below 10% under these standard conditions. A hydrogen/*n*-hexane molar ratio higher than 20 was used to minimize deactivation by coking.

Catalyst pretreatment. Each catalyst was subjected to an aging period. After a pretreatment at 723 K (mordenite and β) or 523 K (ZSM-5 and ZSM-22) in flowing hydrogen the catalyst was submitted to 20 h of standard reaction conditions. During this treatment a deactivation period and a slight increase in the 2-MP/3-MP ratios were observed. All catalysts lost approximately 25% of their initial activity. In the case of β-zeolite, a strong increase in selectivity for dimethylbutanes and a decrease in cracking products were observed. This indicates that deactivation of the metal function is the main reason for the initial deactivation. After stabilization, the catalysts could be used for up to 1000 h on stream without further loss of activity.

Between measurements the catalyst was reactivated by an *in situ* hydrogen pretreatment. This resulted temporarily in an approximately 10% higher activity, which was leveled

TABLE 4

Characterization of the Platinum Function of the *ex Situ* Pretreated Samples

Sample	Liquid phase hydrogenation[a]		Chemisorption
	$qTOF_{Pt}$ [min^{-1}]	X_{dev} [%]	H/Pt
0.5 wt% Pt/HMOR	3.8	75	1.4
1 wt% Pt/HMOR	3.4	55	2.0
2 wt% Pt/HMOR	3.8	40	2.0
3 wt% Pt/HMOR	2.3	80	1.0
1.5 wt% Pt/HBEA	19.8	55	1.6
0.5 wt% Pt/HMFI	19.8	60	1.6
0.7 wt% Pt/HTON	1.8	85	2.0

[a] Solvent *n*-heptane, atmospheric hydrogen pressure, room temperature.

out, depending on the zeolite type, in a 4- to 10-h period. A partial cleaning of the platinum and acid sites was assumed to be responsible for the high initial activity.

Definition of activity. We defined a turnover frequency (TOF) as the number of moles reactant converted per mole of Brønsted acid site per hour. It appeared, however, from our characterization experiments that only one-third of the acid sites in mordenite can be reached by *n*-hexane (20). It might therefore be argued whether in this case the true TOF must be calculated using only one-third of the sites. These values are given in parentheses where needed. On average, the experimental error amounts to 10%.

3. RESULTS

Diffusion Limitations

Experiments using both 0.5 and 2.0 wt% Pt/Hmordenite catalysts showed that external diffusion limitations could be excluded when a total flow of 150 Nml/min was used. Internal diffusion limitations were shown to be irrelevant in experiments using a set of three embedded ZSM-5 samples with crystal sizes ranging from 0.6 to 12 μm. From this we could estimate a lower limit for the effective diffusion coefficient of 8×10^{-14} m^2/s at 513 K (21). This is approximately the same value as obtained by Haag *et al.* at 538 K (22). The same type of experiment was performed on two ZSM-22 catalysts with crystal lengths of 4 (TON(4)) and $\leq 1\mu$m (TON(1)). Here a relative efficiency of 0.28 was found for the larger crystals. This means that, at least for TON(4) crystals, internal diffusion limitations do play a role.

Determination of the Optimum Platinum Loading

Sufficient platinum had to be present to establish the hexane/hexene equilibrium and make the reaction on the acid sites rate determining. The optimum platinum loading was determined by using both *ex situ* pretreated and embedded mordenites as well as two β samples. The relative activities of these catalysts as a function of platinum to acid site ratio are given in Fig. 2.

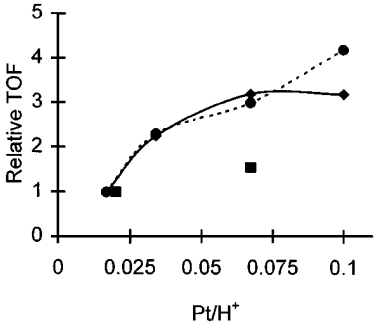

FIG. 2. Relative activity of mordenite catalysts and two β samples as a function of platinum to acid site ratio. (◆) Embedded Mordenite. (●) *Ex situ* pretreated mordenite. (■) *Ex situ* pretreated β-zeolite.

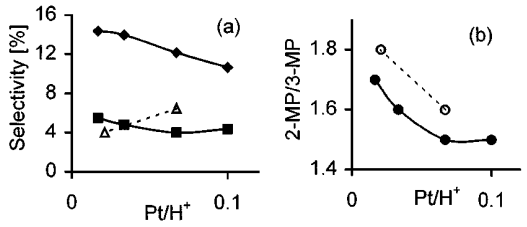

FIG. 3. (a) Selectivities and (b) 2-MP/3-MP ratios on mordenites and two β samples versus platinum to acid site ratio. (■) Hydrocracking (mordenite). (◆) DMBs (mordenite). (△) DMBs (β). (●) 2-MP/3-MP (mordenite). (○) 2-MP/3-MP (β).

In Fig. 3, the hydrocracking selectivity (Fig. 3a) and the 2-methylpentane/3-methylpentane (2-MP/3-MP) ratio (Fig. 3b) are plotted versus the platinum to acid site ratio. The amount of 2,2-dimethylbutane (22-DMB) was very low and difficult to detect (its retention time was almost equal to that of methylcyclopentane, which was a contaminant in the feed *n*-hexane). Therefore, the dimethylbutanes ratio could not always be used as a means to characterize the platinum function. The sum of these products was a more reliable source of information and is also plotted in Fig. 3a. Table 5 lists the kinetic data.

Selectivities

The overall selectivities towards isomerization were usually very high. Only up to 6 mol% cracking products were found at conversions below 10%. ZSM-5 and the 0.5 wt% β even showed an isomerization selectivity of over 99%. However, the isomerization selectivity of the ZSM-22 catalysts was only 80%. In Table 6, the selectivities to the four hexane isomers as a function of zeolite are given at stan-

TABLE 5

Kinetic Data as a Function of Platinum Loading

Zeolite	n^a	m^b	$E_{act,app}$ [kJ/mol]	$E_{act,iso}$ [kJ/mol]
1/2% MOR, embedded	0.42	−0.2	106	122
1% MOR, embedded[c]	0.32	∼0	101	113
2% MOR, embedded	0.24	∼0	111	120
3% MOR, embedded[c]	0.31	−0.23	114	126
1/2% MOR, *in situ*	0.34	∼0	96	109
1% MOR, *in situ*	0.24	0.1	95	104
2% MOR, *in situ*	0.14	∼0	107	112
2% MOR, *ex situ*	0.13	∼0	106	111
3% MOR, *ex situ*	0.19	−0.25	115	122
1/2% BEA, *ex situ*	0.53	−0.24	116	135
1.6% BEA, *ex situ*	0.5[d] (0.69[e])	−0.29	113[d] (99[e])	131[d] (123[e])

[a] 1.95 kPa $< p_{nC_6} <$ 4.29 kPa, $p_{H_2} = 85.7$ kPa.
[b] 68.7 kPa $< p_{H_2} <$ 98.0 kPa, $p_{nC_6} = 3.43$ kPa.
[c] Pretreated at 523 K.
[d] 493 K $< T <$ 506 K.
[e] 493 K $< T <$ 533 K.

TABLE 6

Product Selectivities (mol%) for the "Key" Zeolites at Standard Conditions[a]

Selectivity for	MOR	BEA	TON(1)	TON(4)	MFI (<1 μm)
2-MP	50.5	53.4	55.6	45.4	73.9
3-MP	33.3	34.2	19.5	32.6	22.2
2-MP/3-MP	1.5	1.6	2.9	2.7	3.4
23-DMB	10.5	3.7	0	0	0.3
22-DMB	1.7	2.5	0	0	0
22-DMB/23-DMB	0.2	0.7	n.a.	n.a.	n.a.

Note. n.a., not applicable.

[a] $T = 513$ K, 0.03 ml/min liquid *n*-C_6, 145 Nml/min H_2, conversion $\approx$5%.

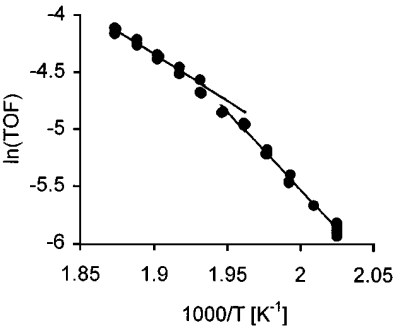

FIG. 4. Arrheniusplot of BEA (1.6 wt% Pt/Hβ). (●) Experimental points, $E_{\text{act, low } T} = 133.3$ kJ/mol, $E_{\text{act, high } T} = 67.3$ kJ/mol.

dard conditions. The 2-MP/3-MP and 2,2-dimethylbutane/2,3-dimethylbutane (22-DMB/23-DMB) ratios are also listed. These ratios are 1.5 and 2.5 at equilibrium respectively. The 2-MP/3-MP ratio increased from 3.4 to 3.6 to 3.8 with increasing MFI crystal diameter. On the TON samples the opposite trend was observed.

Kinetics of the "Key" Samples

All four "key" zeolites had a Pt/H^+ ratio of 0.067. These samples will now be indicated by their IZA three-letter codes (23). Their activities per acid site at standard conditions and the corresponding WHSV as well as the kinetic data are listed in Table 7. All orders of reaction were found to be relatively independent of temperature.

The Arrhenius plot measured on BEA was curved (Fig. 4). In the lower-temperature range (493 to 506 K) the activation energy was 113 kJ/mol, while in the higher-temperature range (521 to 533 K) a value of 67 kJ/mol was obtained. Table 7 contains the low-temperature data.

TABLE 7

Activities under Standard Conditions[a] and Kinetic Data of the "Key" Zeolites

Sample	WHSV [g/gh]	TOF [mol/molh]	n^b	m^c	$E_{\text{act, app}}$ [kJ/mol]	$E_{\text{act, iso}}$ [kJ/mol]
MFI, *ex situ*	12.6	54	0.51	−0.25	103[d]	127
TON(1), *ex situ*	13.5	7.9	0.7	~0	103[d]	136
TON(4), *ex situ*	10.0	2.2	1.0	~0	86[d]	133
MOR, embedded	8.1	9.7 (29.1[e])	0.24	~0	111[d]	120
BEA, *ex situ*	25.9	27.8	0.5[f]	−0.29	113[f]	131

[a] $T = 513$ K, 0.03 ml/min liquid *n*-C_6, 145 Nml/min H_2, conversion $\approx$5%.

[b] 1.95 kPa $< p_{nC_6} <$ 4.29 kPa, $p_{H_2} = 85.7$ kPa.

[c] 68.7 kPa $< p_{H_2} <$ 98.0 kPa, $p_{nC_6} = 3.43$ kPa.

[d] 493 K $< T <$ 533 K.

[e] This takes into account that only one-third of the acid sites can be reached by *n*-C_6.

[f] 493 K $< T <$ 506 K.

4. DISCUSSION

Determination of the Optimum Platinum Loading

The activities of the *ex situ* pretreated and embedded samples were comparable. The *in situ* pretreated samples were less active, which is probably due to the lower dispersion of platinum resulting in rate limitation by the metal function. Since in the latter case the zeolites were pressed into agglomerates before destruction of the platinum complex, the mass transport of the desorbing ammonia will be hindered. This has been shown to lead to low dispersions (13, 24).

Mordenite. In Table 5, the orders of reaction in *n*-hexane for different mordenites are listed. Since these orders are higher on the embedded type catalysts, these mordenites have a smaller active site coverage. On both types a decrease in *n*-hexane orders with increasing loading and a hydrogen order of approximately 0 can be observed up to a platinum content of 2 wt%. The former observation implied that the zeolite coverage and, therefore, the usage of the available acid sites increased. The measured orders agree with Eq. [2] in the case of low hydrogen pressure and high hexane pressure. We found a delicate balance between the rate of the isomerization and deactivation effects. Details of catalyst preparation and pretreatment determine whether the order in hydrogen will be positive or negative.

The solid line (embedded Pt/mordenite) in Fig. 2 shows that the metal function is no longer rate determining at a Pt/H^+ ratio of 0.067. This conclusion is supported by the observed suppression of secondary acid-catalyzed reactions leading to a more bifunctional behavior of the catalyst (25). Moreover, the 2-MP/3-MP ratio decreased with increasing metal loading and reached its equilibrium value at a Pt/H^+ ratio of 0.067.

The dashed line shows a different trend because the 3 wt% sample showed a strong increase in hydro-isomerization activity. We attribute this to local destruction of the mordenite framework caused by growth of large platinum particles (26, 27). The presence of large metal particles was

confirmed by a relatively low H/Pt and a low $qTOF_{Pt}$ in the liquid phase hydrogenation (Table 4). Framework destruction facilitates molecular diffusion or increases the number of reachable acid sites. The former explanation also means that the reaction on the lower loaded samples might be limited by single-file diffusion problems. The decrease of diffusion limitations is evidenced by the value of X_{dev} in the liquid phase hydrogenation. This value decreased with increasing metal loading; the 3 wt% sample showed a higher value.

The orders of reaction also demonstrated that the 3 wt% sample was a special case. Opposite to the trend observed earlier, the *n*-hexane order is higher than that of the 2 wt% sample. Since the hydrogen and *n*-hexane orders are now almost equal, except for the sign, the catalyst shows ideal bifunctional behavior (Eq. [1]) with equilibration between micropore and gas phase. We thus see a change from one extreme at lower loading to another extreme at higher loading.

The true or intrinsic activation energies of isomerization, calculated in Table 5, range from 100 to 125 kJ/mol. When a catalyst does not conform to Eq. [1], the isomerization may not be the (only) rate determining step and Eq. [3] cannot be used. This is the case with the 1 wt% *in situ* pretreated catalyst because of its positive order in hydrogen. In all other cases there seems to be a trend that a low apparent activation energy is "compensated" by a high order in *n*-hexane. This observation is in agreement with Eq. [3]. Still, two sets of intrinsic isomerization activation energies of around 111 and 125 kJ/mol can be distinguished in Table 5.

Kazansky *et al*. calculated by quantum chemistry a value of approximately 120 kJ/mol for the activation energy of deprotonation (dissociation of the alkoxy species) to the adsorbed state (28). We estimated the activation energy of isomerization from the adsorbed state to be approximately 130 kJ/mol (29, 30) and we thus see the same difference in energies (10 kJ/mol) as observed in Table 5. The lower value then represents the activation energy of deprotonation affected by limited hydrogenation activity and the higher value the true intrinsic activation energy of isomerization on a zeolite.

β-Zeolite. A check for the optimum platinum loading was also performed using β-zeolite. The TOF increased by a factor of 1.5, from 0.5 to 1.6 wt% Pt/Hβ (Pt/H^+ ratio of 0.067). This effect was less pronounced than on the mordenite catalyst, which would confirm importance of single-file diffusion on the latter zeolite.

The Arrhenius activation energy changed as a function of temperature for the BEA sample (Fig. 4). This might be explained by a change in coverage of reactive intermediates and thus the order of reaction in *n*-hexane. The assumption of Arrhenius behavior is then no longer valid. The 0.5 wt% Pt/Hβ, however, showed a straight Arrhenius plot. This apparent activation energy is similar to the one obtained on the BEA sample in the lower temperature range (below 518 K). This strongly indicates that the reaction on the higher loaded sample is diffusion limited in the higher temperature range. Since this catalyst is the most active of all (in mol/g · h), this is a real possibility. Falsification of the order in the reactant is a consequence of diffusion limitations (31):

$$n_{observed} = n_{true} + \frac{n_{true} - 1}{2} \frac{d \ln \eta}{d \ln \phi} \qquad [4]$$

Since $d \ln \eta / d \ln \phi$ has a value between 0 and −1, and order will be observed that is higher than the true order. Measurements indeed showed a higher order at higher loading.

The 2-MP/3-MP ratio selectivity decreased at increasing platinum loading. An opposite trend was observed for the sum of the dimethylbutanes which was mainly due to an increase in 22-DMB. According to Blomsma *et al*., 22-DMB cannot be formed by a dimerization and cracking mechanism and can, therefore, be used to monitor monomolecular activity versus bimolecular activity on β-zeolite (32). Our observation is in favor of an increase of the former mechanism. The cracking activity increased from a 0.5 to a 1.6 wt% Pt/β. This was mainly due to an increase in acid cracking. This is possibly due to the high residence times caused by diffusion limitations.

The "Key" Zeolites

Activity. When adsorption effects play a decisive role in determining the activity, MOR and BEA should be equally active. The same must be true for MFI and TON. BEA is, however, three times more active than MOR (Table 7). When one corrects for only one-third usage of the acid sites in MOR, the BEA and MOR are equally active. MOR might, however, experience single-file diffusion problems. On the other hand, we discussed that the reaction on BEA is probably diffusion limited at 513 K. The *ex situ* pretreated 3 wt% Pt/H mordenite has an approximately $1\frac{1}{2}$ times higher TOF than the MOR catalyst, which still cannot account for the factor of three difference in activity. The low noncorrected TOF of MOR then indicates that both site accessibility and diffusion play a role.

The TON(4) samples are very inactive compared to MFI. This is consistent with pore-mouth catalysis. This phenomenon was first proposed by Martens *et al*. on the basis of the peculiar isomerization selectivity of this zeolite in the reaction of *n*-decane and Molecular graphics calculations (33). Pore-mouth catalysis means that only part of the sites is taking part in the reaction and is in fact an extreme case of single-file diffusion limitation. Indeed the TON(1) crystals are almost 4 times more active than the TON(4) crystals, which would be consistent. The activity of TON(1) is, however, still not as high as would be expected from its adsorption enthalpy. Assuming that the activity per active site of TON is equal to that of MFI, the sites that contribute to

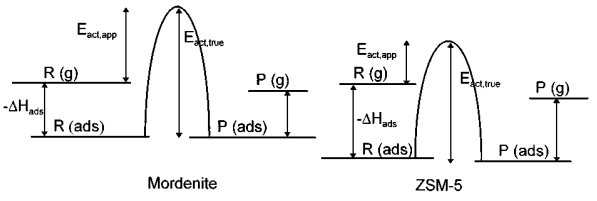

FIG. 5. Energy scheme of true and apparent activation energies ($\theta \approx 0$). $E_{\text{act, app}}$, apparent activation energy; $E_{\text{act, true}}$, true activation energy; ΔH_{ads}, enthalpy of adsorption; R(g), gas phase reactant; R(ads), adsorbed reactant; P(g), gas phase product; P(ads), adsorbed product.

the activity can be estimated. Only 4% of the acid sites are then active on the 4 μm crystals; for the 1-μm crystals this is 15%.

Table 7 shows that the TOF of MFI is a factor of 5 ($1\frac{1}{2}$) higher than for MOR and a factor of $1\frac{1}{2}$ higher than for BEA. It may be concluded that a higher adsorption enthalpy leads to a higher activity, as long as one excludes the TON data. This phenomenon might be explained as is schematically shown in Fig. 5 for an almost empty zeolite. The true activation energy of isomerization is the same for all zeolites. Equation [3] and Table 7 also show that, for the same order of reaction, the apparent activation energy for isomerization is lowest using the highest adsorption enthalpy (MFI). Kinetic computer simulations, published elsewhere, led to the same conclusion (7). The overall effect will be small due to the low orders in the reactant.

Selectivity of the medium pore zeolites. The MFI and TON catalysts showed product shape selectivity since the DMBs were formed in very low quantities (if any). Also the 2-MP/3-MP ratio was far from equilibrium on both catalysts and might be explained in two ways:

1. 3-MP is just a little bit bulkier than 2-MP. The effective size of 3-MP (4.4×5.8 Å) is very close to that of a ZSM-5 pore (5.3×5.6 Å or 5.1×5.5 Å) (22). From its structure one expects 2-MP to be smaller.

2. Monobranched products can only adsorb with the linear part of the chain into the TON catalyst (33, 34). This results in a higher adsorption enthalpy for 2-MP than for 3-MP.

Since the 2-MP/3-MP ratio increased on MFI and decreased on TON with increasing crystal size, two different mechanisms must be operable to establish the relatively high 2-MP/3-MP ratios. A size effect (explanation 1) is more probable on MFI since it is increasingly difficult for the bulkier product to diffuse out of a crystal at increasing crystal size. Explanation 2 is more pronounced on TON since larger crystals possess fewer pore mouths to perform the reaction.

Another special feature of the TON-type catalysts is the low isomerization selectivity. This might be due to pore-mouth reaction or high residence times. The platinum is highly dispersed inside the zeolite crystals, as evidenced by a high H/Pt (Table 4) and a low qTOF_{Pt} (due to diffusion problems). The metal particles are, therefore, difficult to reach by the reactant and an acid (cracking) mechanism is observed: the main cracking product is propane (4). When, however, the platinum is poorly dispersed very high isomerization selectivities can be obtained (34). Either explanation can account for the lowered cracking on the smaller TON crystals.

Selectivity of the large pore zeolites. MOR and BEA converted *n*-hexane to the MPs in their equilibrium ratio. The selectivity toward 22-DMB was low since the formation of this isomer involves a secondary carbenium ion, through either isomerization of monomethylpentanes or a methyl shift of 23-DMB (35). Formation of the latter involves a tertiary carbenium ion. 22-DMB can even be formed by direct transformation of *n*-hexane when the reactant is isomerized twice before it is hydrogenated on the platinum. This may be the case at low platinum loading or zeolites with a one-dimensional pore system, such as mordenite (36).

Orders of reaction. The two zeolites with a three-dimensional pore system, BEA and MFI, showed similar orders. The order of reaction in *n*-hexane of 0.69 measured on BEA might be obtained under external diffusion limited conditions. The fact that the absolute value of the order in hydrogen is lower than the order in *n*-hexane is not consistent with either Eq. [1] or [2]. Since we found the same phenomenon in our kinetic simulations that did not contain deactivation, deactivation does not have to be invoked as an explanation. We believe from the simulations that slow hydrogenation of the isomer hexenes is a more probable explanation (7).

The TON(4) sample appeared to be almost empty, since the order of reaction in *n*-hexane in this case was 1. Considering the high adsorption enthalpy we believe that the zeolite was actually almost completely filled and most sites were blocked by reactant molecules. Hence only a few sites were responsible for the reaction, which supported the conclusion of pore-mouth catalysis. The order in *n*-hexane on the TON(1) sample was lower, which indicated that more sites are used in this reaction. This enhanced usage of acid sites was already calculated from the activity data. Using $\theta_{n\text{-alkoxy}} \approx 1 - n$, coverages of 0 and 30% can be estimated. From the activity data values of respectively 4 and 15% were calculated. This is a reasonable agreement considering the crudeness of estimation.

Activation energies. The measurements listed in Table 7 showed that increasing adsorption enthalpy of a zeolite led to lower apparent activation energy and higher activity. We already concluded in the discussion for the optimum platinum content that the intrinsic activation energy on a zeolite is approximately 125 kJ/mol. This value is confirmed by Table 7. The thus calculated true activation energy of

isomerization is much higher than the one in the superacid solution (approximately 30 kJ/mol) (30). This is due to the fact that in reactions catalyzed by acidic zeolites alkoxy species are the reactive intermediates. The covalent C–O bond between carbon chain and zeolite lattice must be (partially) dissociated before isomerization.

5. CONCLUSIONS

Differences in activity of different zeolites are due not only to differences in intrinsic acid strength but also to a combination of adsorption and diffusion effects. We demonstrated this using four zeolites that were intrinsically equally acidic. Their activities per acid site could be therefore be directly compared. A higher adsorption enthalpy led to a lower apparent activation energy and, thus, a higher activity per acid site. On the zeolites under investigation the activation energy of the elementary isomerization reaction with respect to a *n*-alkoxy intermediate was the same for all structures and amounted to approximately 125 kJ/mol. This value is much higher than in the superacid solution because of the energy needed to break or lengthen the bond between the alkoxy carbon and zeolite lattice oxygen.

ZSM-22 showed pore-mouth catalysis due to its one-dimensional pore system with relatively small pores. This zeolite was therefore relatively inactive. Both ZSM-5 and ZSM-22 showed shape selectivity while no dimethylbutanes were formed and the 2-MP/3-MP ratio was not at equilibrium. The latter was at equilibrium on both large-pore zeolites, mordenite and β. The reaction on β-zeolite may have become diffusion limited at higher temperatures due to its high activity per gram. The mordenite data indicate the possibility of single-file diffusion and a limited accessibility of the acid sites.

ACKNOWLEDGMENT

The work described in this paper was funded by the Dutch Organization for Scientific Research (NWO) through its Foundation for Chemistry (SON).

REFERENCES

1. Weisz, P. B., *in* "Advances in Catalysis and Related Subjects, Vol. 13" (D. D. Eley, P. W. Selwood, and P. B. Weisz, Eds.), p. 157. Academic Press, London, 1963.
2. Kazansky, V. B., *in* "Acidity and Basicity of Solids, Theory, Assessment and Utility" (J. Fraissard and L. Petrakis, Eds.), p. 335. Kluwer Academic, Dordrecht, 1994.
3. Kazansky, V. B., and Senchenya, I. N., *J. Catal.* **119**, 108 (1989).
4. Ribeiro, F., Marcilly, C., and Guisnet, M., *J. Catal.* **78**, 267 (1982).
5. Steijns, M., and Froment, G. F., *Ind. Eng. Chem. Prod. Res. Dev.* **4**, 660 (1981).
6. Froment, G. F., *Catalysis Today* **1**, 455 (1987).
7. Van de Runstraat, A., Van Grondelle, J., and Van Santen, R. A., *Ind. Eng. Chem. Res.*, in press.
8. Van Santen, R. A., and Niemantsverdriet, J. W., "Chemical Kinetics and Catalysis," p. 49. Plenum Press, New York, 1995.
9. Stach, H., Lohse, U., Thamm, H., and Schirmer, W., *Zeolites* **6**, 74 (1986).
10. Lerchert, H., and Schweitzer, W., *in* "Proceedings of the International Conference on Zeolites, Reno" (D. Olson and A. Bisio, Eds.), p. 210. Guildford-Butterworth, 1983.
11. "API 44 Tables," American Petroleum Institute Research Project, Vols. V and VI, Thermodynamic Research Center, Texas A&M University, 1968.
12. Kazansky, V. B., Frash, M. V., and Van Santen, R. A., *Appl. Catal.* **146**, 225 (1996).
13. Van den Broek, A. C. M., Van Grondelle, J., and Van Santen, R. A., *J. Catal.* **167**, 417 (1997).
14. Jänchen, J., Van Wolput, J. H. M. C., Van de Ven, L. J. M., De Haan, J. W., and Van Santen, R. A., *Catal. Lett.* **39**, 147 (1996).
15. Bates, S. P., and Van Santen, R. A. [Unpublished results]
16. Meier, W. M., Olson, D. H., and Baerlocher, Ch., "Atlas of Zeolite Structure Types." Elsevier, Amsterdam, 1996.
17. Jänchen, J., Stach, H., Uytterhoeven, L., and Mortier, W. J., *J. Phys. Chem.* **100**, 12489 (1996).
18. Eder, F. [Personal communication]
19. Madon, R. J., O'Conell, J. P., and Boudart, M., *AIChE* **24**, 904 (1978).
20. This conclusion is supported by: Stockenhuber, M., Eder, F., and Lercher, J. A., *Stud. Surf. Sci. Catal.* **97**, 495 (1995).
21. Van der Pol, A. J. H. P., Verduyn, A. J., and Van Hooff, J. H. C., *Appl. Catal.* **92**, 113 (1992).
22. Haag, W. O., Lago, R. M., and Weisz, P. B., *Faraday Disc. Chem. Soc.* **72**, 317 (1982).
23. Meier, W. M., Olson, D. H., and Baerlocher, Ch., "Atlas of Zeolite Structure Types," Elsevier, Amsterdam/New York, 1996.
24. Sachtler, W. M. H., and Zhang, Z., *Adv. Catal.* **39**, 129 (1993).
25. Gianetto, G., Alvares, F., Ribeiro, F. R., Pérot, G., and Guisnet, M., *in* "Guidelines for Mastering the Properties of Molecular Sieves" (D. Barthomeuf, E. G. Derouane, and W. Hölderich, Eds.), NATO ASI Series B, Vol. 221, p. 355. Plenum Press, New York, 1990.
26. Carvill, B. T., Lerner, B. A., Adelman, B. J., Tomczak, D. C., and Sachtler, W. M. H., *J. Catal.* **144**, 1 (1993).
27. Jaeger, N. I., Jaeger, A. L., and Schulz-Ekloff, G., *J. Chem. Soc. Faraday Trans.* **87**, 1251 (1991).
28. Kazansky, V. B., Frash, M. V., and Van Santen, R. A., *Appl. Catal.* **146**, 225 (1996).
29. Van de Runstraat, A., Stobbelaar, P. J., Van Grondelle, J., Anderson, B. G., Van IJzendoorn, L. J., and Van Santen, R. A., *Stud. Surf. Sci. Catal.* **105**, 1253 (1996).
30. Brouwer, D. M., *in* "Chemistry and Chemical Engineering of Catalytic Processes" (G. C. A. Schuit and R. Prins, Eds.), p. 137. Noordhoff, Alphenaanden Rijn, Rockville, MD, 1980.
31. Languasco, J. M., Cunningham, R. E., and Calvelo, A., *Chem. Eng. Sci.* **27**, 1459 (1972).
32. (a) Blomsma, E., Martens, J. A., and Jacobs, P. A., *J. Catal.* **155**, 141 (1995); (b) Blomsma, E., Martens, J. A., and Jacobs, P. A., *J. Catal.* **159**, 323 (1996); (c) Blomsma, E., Martens, J. A., and Jacobs, P. A., *Stud. Surf. Sci. Catal.* **105**, 909 (1996).
33. Martens, J. A., Parton, R., Uytterhoeven, L., Jacobs, P. A., and Froment, G. F., *Appl. Catal.* **76**, 95 (1991).
34. Martens, J. A., Souverijns, W., Verrelst, W., Parton, R., Froment, G. F., and Jacobs, P. A., *Angew. Chemie* **107**, 2726 (1995).
35. (a) Li, C., and Zhu, Z., *Fuel Sci. Technol.* **9**, 1103 (1991); (b) Marin, G. B., and Froment, G. F., *Chem. Eng. Sci.* **37**, 759 (1982).
36. Allain, J. F., Magnoux, P., Schulz, Ph., and Guisnet, M., *in* "Proceedings of the DGMK-Conference: Catalysis on Solid Acid and Bases" (J. Weitkamp and B. Lücke, Eds.), p. 219. German Society for Petroleum and Coal Science and Technology, 1996.